Carbon Dioxide Mediated Synthesis of Mesoporous Silica Films: Tuning Properties using Pressure

Xinxin Li and Bryan D. Vogt*

Department of Chemical Engineering, Arizona State University, Tempe, Arizona 85284

Received February 3, 2008. Revised Manuscript Received February 29, 2008

Mesoporous silica films were synthesized by the selective condensation of tetraethylorthosilicate (TEOS) within preformed amphiphilic templates using carbon dioxide as a carrier for the precursor. Blends of poly(ethylene oxide)-*b*-poly(propylene oxide)-*b*-poly(ethylene oxide) (Pluronic F108) and poly(*p*-hydroxystyrene) (PHOSt) containing *p*-toluenesulfonic acid were exposed to gaseous or supercritical fluid solutions of CO_2, TEOS, and H_2O at 60 °C. The subsequent sorption within the polymeric template delivered the precursors for selective reaction in the hydrophilic domains. Mesoporous silica films were formed by the removal of the template by calcination at 450 °C. The physical properties of mesoporous silica were tailored through control of the CO_2 pressure during the reaction. The pore size increased slightly (1.6−1.81 nm) as the CO_2 pressure was increased to 80 bar. A small increase in pressure resulted in a significant expansion of the pore size near 84 bar to nearly 4 nm pore radii. In addition to tuning the mesopore size, increasing the CO_2 pressure during synthesis led to a decrease in the apparent reaction rate and subsequently an increase in the film porosity. Moreover, the apparent accessibility of the mesopores to small molecules as evidenced by the lack of capillary condensation of water and toluene was tuned by the CO_2 pressure. Synthesis very near the critical pressure of CO_2 resulted in a small fraction of the pores being accessible. Thus, synthesis of mesoporous films using CO_2 appears to be a promising route to limit the contamination of low-*k* dielectric materials for microelectronics applications.

Introduction

The templated synthesis of mesoporous materials based on the cooperative assembly of structure-directing surfactants and network-forming precursors[1,2] has emerged as a facile route for the design of tunable nanostructured materials. These methods generally yield highly ordered periodic mesoporous materials, whose morphology can be controlled through the choice of surfactant, solution concentration, and solution conditions (temperature and pH).[3–6] Potential applications for mesoporous films include photovoltaic devices,[7] catalysis,[8] separation membranes,[9] sensors,[10] and low-*k* dielectric for microelectronics.[11] The utility of a given mesoporous film depends upon its physicochemical properties generally including pore wall chemistry,[12] pore morphology,[3] porosity,[4] pore size distribution,[13] and mechanical robustness.[14] For sol–gel processing of mesoporous materials, tremendous efforts have been extendent on improving these properties through processing.[15,16] These efforts have identi-

* To whom correspondence should be addressed. E-mail: bryan.vogt@asu.edu.

(1) Kresge, C. T.; Leonowicz, M. E.; Roth, W. J.; Vartuli, J. C.; Beck, J. S. Ordered mesoporous molecular-sieves synthesized by a liquid-crystal template mechanism. *Nature (London, U.K.)* **1992**, *359* (6397), 710–712.

(2) Beck, J. S.; Vartuli, J. C.; Roth, W. J.; Leonowicz, M. E.; Kresge, C. T.; Schmitt, K. D.; Chu, C. T. W.; Olson, D. H.; Sheppard, E. W.; Mccullen, S. B.; Higgins, J. B.; Schlenker, J. L. A new family of mesoporous molecular-sieves prepared with liquid-crystal templates. *J. Am. Chem. Soc.* **1992**, *114* (27), 10834–10843.

(3) Alberius, P. C. A.; Frindell, K. L.; Hayward, R. C.; Kramer, E. J.; Stucky, G. D.; Chmelka, B. F. General predictive syntheses of cubic, hexagonal, and lamellar silica and titania mesostructured thin films. *Chem. Mater.* **2002**, *14* (8), 3284–3294.

(4) Imperor-Clerc, M.; Davidson, P.; Davidson, A. Existence of a microporous corona around the mesopores of silica-based SBA-15 materials templated by triblock copolymers. *J. Am. Chem. Soc.* **2000**, *122* (48), 11925–11933.

(5) Kruk, M.; Jaroniec, M.; Ko, C. H.; Ryoo, R. Characterization of the porous structure of SBA-15. *Chem. Mater.* **2000**, *12* (7), 1961–1968.

(6) Galarneau, A.; Cambon, H.; Di Renzo, F.; Fajula, F. True microporosity and surface area of mesoporous SBA-15 silicas as a function of synthesis temperature. *Langmuir* **2001**, *17* (26), 8328–8335.

(7) Coakley, K. M.; McGehee, M. D. Photovoltaic cells made from conjugated polymers infiltrated into mesoporous titania. *Appl. Phys. Lett.* **2003**, *83* (16), 3380–3382.

(8) Corma, A. From microporous to mesoporous molecular sieve materials and their use in catalysis. *Chem. Rev.* **1997**, *97* (6), 2373–2419.

(9) Lai, Z. P.; Bonilla, G.; Diaz, I.; Nery, J. G.; Sujaoti, K.; Amat, M. A.; Kokkoli, E.; Terasaki, O.; Thompson, R. W.; Tsapatsis, M.; Vlachos, D. G. Microstructural optimization of a zeolite membrane for organic vapor separation. *Science (Washington, DC, U.S.)* **2003**, *300* (5618), 456–460.

(10) Stein, A. Advances in microporous and mesoporous solids−Highlights of recent progress. *Adv. Mater.* **2003**, *15* (10), 763–775.

(11) Yang, S.; Mirau, P. A.; Pai, C.-S.; Nalamasu, O.; Reichmanis, E.; Lin, E. K.; Lee, H.-J.; Gidley, D. W.; Sun, J. Molecular templating of nanoporous ultralow dielectric constant (∼1.5) organosilicates by tailoring the microphase separation of triblock copolymers. *Chem. Mater.* **2001**, *13*, 2762–2764.

(12) Yang, P. D.; Zhao, D. Y.; Margolese, D. I.; Chmelka, B. F.; Stucky, G. D. Generalized syntheses of large-pore mesoporous metal oxides with semicrystalline frameworks. *Nature (London, U.K.)* **1998**, *396* (6707), 152–155.

(13) Fang, H.; Zhang, M.; Shi, W. H.; Wan, T. L. Facile synthesis of ordered large-pore mesoporous silica thin film with *Im*3*m* symmetry using *n*-butanol as the cosurfactant. *J. Non-Cryst. Solids* **2006**, *352* (21–22), 2279–2283.

(14) Fan, H.; Hartshorn, C.; Buchheit, T.; Tallant, D.; Assink, R. A.; Simpson, R.; Kissel, D. J.; Lacks, D. J.; Torquato, S.; Brinker, C. J. Modulus density scaling behavior and framework architecture of nanoporous self-assembled silicas. *Nat. Mater.* **2007**, *6*, 418–423.

(15) Barton, T. J.; Bull, L. M.; Klemperer, W. G.; Loy, D. A.; McEnaney, B.; Misono, M.; Monson, P. A.; Pez, G.; Scherer, G. W.; Vartuli, J. C.; Yaghi, O. M. Tailored porous materials. *Chem. Mater.* **1999**, *11* (10), 2633–2656.

10.1021/cm8003479 CCC: $40.75
Published on Web 04/18/2008

fied several key processing variables including humidity during drying[17] and postsynthesis aging[18] for controlling the final structure of the mesoporous films.

More recently, alternative synthetic approaches were developed that utilize preformed template films and introduce the reactive precursors either through vapor (utilizing the vapor pressure of the precursors)[19–21] or through supercritical fluid (dissolving the precursors in CO_2)[22,23] phases. These synthetic routes have a number of potential advantages over the traditional solution-phase synthesis. First, the simultaneous cooperative assembly and precursor condensation during typical sol based syntheses can impede the formation of long-range order and the desired pore orientation, which are crucial for a number of applications. Second, the requirements of mutual solubility and specific interactions for cooperative assembly are relaxed for the preformed templates as the self-assembly and inorganic network formation is fully decoupled. This decoupling of structure-forming processes can improve control of the long-range order and orientation of the mesopores.[22] Recently, Watkins and co-workers reported that the addition of an associating homopolymer (through hydrogen bonding) to common poly(ethylene oxide) based amphiphilic templates, such as Pluronic and Brij surfactants, dramatically increased the long-range order of the mesostructure.[24] The best ordered materials were found using a homopolymer,[24] poly(hydroxystyrene), that is not soluble in typical acidic sols for the synthesis of mesoporous materials.[25] Thus, these templates are limited to either the vapor or the supercritical fluid synthesis routes. Moreover, this long-range order significantly increases the mechanical robustness of the film.[26]

However, the impact on physical properties of using CO_2 in comparison to the vapor pressure of the precursors for the synthesis of mesoporous materials has not been investigated thoroughly. The reaction−diffusion processes of metal oxide network formation in the preformed templates can suffer from transport limitations of the precursors in the bulk polymer. These transport limitations can be overcome by swelling the copolymer with supercritical CO_2 (SC-CO_2), which increases the diffusivity of small molecules by several orders of magnitude.[23] But, films over 300 nm thick have been synthesized using the vaporized approach with no mention of film thickness limitations.[19] However, in the vapor pressure based synthesis, a surface coating of apparently dense silica occurs[21] either from homogeneous nucleation (using the vapor pressure of a mineral acid, HCl, as a catalyst for hydrolysis) or diffusion limitations through the polymer film. Conversely, for films synthesized using SC-CO_2, a homogeneous ordered porous film is formed even for films more than 1 μm thick.[22] Therefore, synthesis using SC-CO_2 provides a processing advantage for film uniformity.

To date, reports on the synthesis of mesoporous films utilizing SC-CO_2 have been limited primarily to demonstrations of the technique[22,23] or the resulting morphology.[27] Investigations of the influence of SC-CO_2 during synthesis on the properties of these mesoporous films are presently lacking. However, the postprocessing of condensed ordered mesostructured nanocomposites with SC-CO_2 has been reported recently as a route to control the pore size of the resulting mesoporous material.[28–30] In this case, CO_2 acts as a swelling agent and expands the organic domains, leading to an increase in pore size. The pore size and *d*-spacing of the mesoporous silica increase almost linearly as the CO_2 pressure increases.[28–30] It is expected that the presence of CO_2 during the condensation reaction will lead to deviations from a simple linear increase in the pore size with pressure. Instead, CO_2 likely impacts numerous properties of the films; for example, the microporosity of CO_2 synthesized mesoporous organosilicate films[27] is significantly larger than that observed for vapor-phase infused mesoporous silicates.[26]

Numerous methods have been utilized or developed for the characterization of mesoporous films. Properties that are generally quantified for these films include pore morphology, porosity, pore size distribution, and the modulus. These properties are interrelated to each other and the specifics of the processing. Typical characterization for mesoporous powders include X-ray diffraction (XRD), transmission electron microscopy (TEM), thermogravimetric analysis

(16) Brinker, C. J.; Dunphy, D. R. Morphological control of surfactant-templated metal oxide films. *Curr. Opin. Colloid Interface Sci.* **2006**, *11* (2–3), 126–132.
(17) Urade, V. N.; Wei, T. C.; Tate, M. P.; Kowalski, J. D.; Hillhouse, H. W. Nanofabrication of double-gyroid thin films. *Chem. Mater.* **2007**, *19* (4), 768–777.
(18) Urade, V. N.; Hillhouse, H. W. Synthesis of thermally stable highly ordered nanoporous tin oxide thin films with a 3-D face-centered orthorhombic nanostructure. *J. Phys. Chem. B* **2005**, *109* (21), 10538–10541.
(19) Nishiyama, N.; Tanaka, S.; Egashira, Y.; Oku, Y.; Ueyama, K. Vapor-phase synthesis of mesoporous silica thin films. *Chem. Mater.* **2003**, *15* (4), 1006–1011.
(20) Tanaka, S.; Nishiyama, N.; Oku, Y.; Egashira, Y.; Ueyama, K. Nano-architectural silica thin films with two-dimensionally connected cage-like pores synthesized from the vapor phase. *J. Am. Chem. Soc.* **2004**, *126* (15), 4854–4858.
(21) Tanaka, S.; Tate, M. P.; Nishiyama, N.; Ueyama, K.; Hillhouse, H. W. Structure of mesoporous silica thin films prepared by contacting PEO_{106}-PPO_{70}-PEO_{106} films with vaporized TEOS. *Chem. Mater.* **2006**, *18* (23), 5461–5466.
(22) Pai, R. A.; Humayun, R.; Schulberg, M. T.; Sengupta, A.; Sun, J. N.; Watkins, J. J. Mesoporous silicates prepared using preorganized templates in supercritical fluids. *Science (Washington, DC, U.S.)* **2004**, *303*, 507–510.
(23) Pai, R. A.; Watkins, J. J. Synthesis of mesoporous organosilicate films in supercritical carbon dioxide. *Adv. Mater.* **2006**, *18* (2), 241–245.
(24) Tirumala, V. R.; Pai, R. A.; Agaarwal, S.; Testa, J. J.; Bhatnagar, G.; Romany, A. H.; Chandler, C.; Gorman, B. P.; Jones, R. L.; Lin, E. K.; Watkins, J. J. Mesoporous silica films with long-range order prepared from strongly segregated block copolymer/homopolymer blend templates. *Chem. Mater.* **2007**, *19* (24), 5868–5874.
(25) Zhao, D. Y.; Huo, Q. S.; Feng, J. L.; Chmelka, B. F.; Stucky, G. D. Nonionic triblock and star diblock copolymer and oligomeric surfactant syntheses of highly ordered, hydrothermally stable, mesoporous silica structures. *J. Am. Chem. Soc.* **1998**, *120* (24), 6024–6036.
(26) Li, X.; Song, L.; Vogt, B. D. Tuning mechanical properties of mesoporous silicas using associating homopolymers/block copolymer blends as templates. *J. Phys. Chem. C* **2008**, *112* (1), 53–60.
(27) Vogt, B. D.; Pai, R. A.; Lee, H. J.; Hedden, R. C.; Soles, C. L.; Wu, W. L.; Lin, E. K.; Bauer, B. J.; Watkins, J. J. Characterization of ordered mesoporous silica films using small-angle neutron scattering and X-ray porosimetry. *Chem. Mater.* **2005**, *17* (6), 1398–1408.
(28) Hanrahan, J. P.; Copley, M. P.; Ryan, K. M.; Spalding, T. R.; Morris, M. A.; Holmes, J. D. Pore expansion in mesoporous silicas using supercritical carbon dioxide. *Chem. Mater.* **2004**, *16* (3), 424–427.
(29) Hanrahan, J. P.; Copley, M. P.; Ziegler, K. J.; Spalding, T. R.; Morris, M. A.; Steytler, D. C.; Heenan, R. K.; Schweins, R.; Holmes, J. D. Pore size engineering in mesoporous silicas using supercritical CO_2. *Langmuir* **2005**, *21* (9), 4163–4167.
(30) Ghosh, K.; Vyas, S. M.; Lehmler, H. J.; Rankin, S. E.; Knutson, B. L. Tailoring porous silica films through supercritical carbon dioxide processing of fluorinated surfactant templates. *J. Phys. Chem. B* **2007**, *111* (2), 363–370.

(TGA), and N_2 (BET) adsorption.[4–6,12,31] However, the latter two techniques are not readily adapted to the characterization of thin films; thus, alternatives, especially for determining the pore size distribution (PSD) of thin films, have been developed. The porosity of thin films can be obtained from ellipsometric porosimetry (EP), X-ray porosimetry (XRP), Positron annihilation spectroscopy (PAS/PALS), surface acoustic wave spectroscopy (SAWS), and traditional N_2 adsorption with reasonable agreement between the techniques.[32,33]

Although the adsorption phenomenon is complex, it has emerged as the standard technique to probe PSD of materials; thus, adsorption based methods for thin films are desired. N_2 adsorption into thin films also has been used to calculate PSD by measuring the scattering changes using small angle neutron scattering (SANS).[34] However, the wall material must be matched by the neutron scattering length density (NSLD) for the adsorbed nitrogen for tractable analysis. For a more generalized analysis, the SANS contrast variation was used to characterize the PSD of low-*k* dielectrics.[35] In this case, toluene vapor was used instead of N_2 as the pore filling agent, as the NSLD for organic compounds can be controlled by selective deuteration.[27,36] Similar to this approach to determine the PSD of films, Baklanov and co-workers developed a probe based technique similar in kind to N_2 BET adsorption except that instead of pressure decay, changes in the optical constants for the film were measured.[37] This technique, ellipsometric porosimetry (EP), utilizes accuracy in determining the optical properties of thin films by ellipsometry coupled with capillary condensation[38] of a probe molecule, typically water or toluene.

In this study, the influence of SC-CO_2 processing during synthesis of mesoporous silica on the porosity and pore size distribution was determined using EP. The pressure of CO_2 during synthesis was varied from zero to well above P_c. Additional structural characterizations (TEM and XRD) were utilized to provide complementary characterization. This systematic study quantifies the impact of CO_2 on the synthesis of mesoporous silica using preformed templates.

Experimental Procedures

Materials and Synthesis. Polymer templates were prepared from solutions containing poly(ethylene oxide)-*b*-poly(propylene oxide)-*b*-poly(ethylene oxide) (Pluronic F108, BASF), poly(*p*-hydroxystyrene) (PHOSt, $M_n = 8000$ g/mol, DuPont Electronic Materials), and *p*-toluenesulfonic acid (p-TSA, Aldrich) dissolved in a mixture of ethanol (Aldrich) and deionized water with a weight ratio of 0.85 F108/0.15 PHOSt/0.05 p-TSA/9 EtOH/3.6 H_2O. PHOSt acts to increase the degree of segregation of Pluronic,[24] while p-TSA acts as the acid catalyst. p-TSA is used in place of a typical mineral acid such as HCl to avoid any ambiguities from homogeneous hydrolysis in the fluid phase as the vapor pressure of p-TSA is negligible. Silicon wafers were utilized as substrates and were cleaned using piranha solution (3:7 35 wt % hydrogen peroxide/98 wt % sulfuric acid) at 90 °C for 20 min prior to film formation. Template films were spin coated (2000 rpm, 55 s) on the clean substrates. All template films after spin coating had a nominal thickness of 590 nm.

Mesoporous silica films were synthesized in a closed stainless steel vessel (25 mL, Thar) preheated to 60 °C. A fixed quantity of precursors (10 μL of tetraethylorthosilicate (TEOS, Aldrich) and 20 μL of deionized water) was used for all syntheses. For vapor-phase condensation ($P = 0$), no CO_2 was added, and the reaction was allowed to proceed via the vapor pressure of the precursors. Otherwise, the vessel was pressurized slowly with CO_2 to the desired pressure. All the reactions were allowed to proceed for 30 min, and then the reactor was depressurized slowly to atmospheric pressure. A postsynthesis aging in a sealed vessel with saturated water vapor at 90 °C for 2 h was used to enhance the silica network formation. The template was removed via calcination at 450 °C for 5 h at a heating rate of 1 °C/min in air to yield a mesoporous silica film.

Film Characterization. XRD and TEM were utilized to characterize the film morphology. XRD data were collected using a Bruker D8 diffractometer with Cu Kα ($\lambda = 0.15418$ nm) radiation in a $\theta/2\theta$ geometry over an angular range between 0.5 and 5° with an increment of 0.01° on calcined films. Diffraction peaks were indexed to assign the film space group. The primary *d*-spacing was calculated using Bragg's law while correcting for the critical angle of the sample due to the low diffraction angles for the mesopores.[21] TEM micrographs were obtained using a JEOL 2010F instrument operating at 200 keV. TEM cross-sections were prepared by manual polishing of a cut section of the film/substrate.

Ellipsometry was used to characterize the evolution of the film thickness and refractive index after several processing steps with a UV–vis-NIR (240–1700 nm) variable angle spectroscopic ellipsometer (VASE M-2000, J. A. Woollam Co.). For general characterization, a wavelength range from 245 to 1700 nm and three incident angles, 65, 70, and 75°, were used. The Cauchy model was found to effectively approximate the optical properties of the polymeric template, the silica-polymer nanocomposite after reaction, and the mesoporous film. An effective medium approximation (EMA) model was used to calculate the film porosity (P). This model assumes that the mesoporous film consists of a silica framework and voids with an assumed fixed refractive index for the glass silica skeleton.[39]

The pore size distribution (PSD) of the film was determined using EP utilizing toluene (Aldrich) as the probe solvent. The partial

(31) Zhao, D. Y.; Feng, J. L.; Huo, Q. S.; Melosh, N.; Fredrickson, G. H.; Chmelka, B. F.; Stucky, G. D. Triblock copolymer syntheses of mesoporous silica with periodic 50 to 300 Å pores. *Science (Washington, DC, U.S.)* **1998**, *279* (5350), 548–552.
(32) Baklanov, M. R.; Kondoh, E.; Lin, E. K.; Gidley, D. W.; Lee, H.-J.; Mogilnikov, K. P.; Sun, J. N. Comparative study of porous SOG films with different non-destructive instrumentation. *Proc. Intl. Interconnect Technol. Conf.* **2001**, *4*, 189–191.
(33) Baklanov, M. R.; Mogilnikov, K. P. Non-destructive characterization of porous low-*k* dielectric films. *Microelectron. Eng.* **2002**, *64* (1–4), 335–349.
(34) Smarsly, B.; Goltner, C.; Antonietti, M.; Ruland, W.; Hoinkis, E. SANS investigation of nitrogen sorption in porous silica. *J. Phys. Chem. B* **2001**, *105*, 831–840.
(35) Hedden, R. C.; Lee, H.-J.; Bauer, B. J.; Soles, C. L.; Wu, W.; Lin, E. K. Measurement of Pore Size and Matrix Characteristics in Low-*k* Dielectrics by Neutron Contrast Variation. In *Proceedings of the International Conference on Characterization and Metrology for ULSI Technology*, Austin, TX, 2003.
(36) Hedden, R. C.; Lee, H. J.; Bauer, B. J. Characterization of nanoporous low-*k* thin films by small-angle neutron scattering contrast variation. *Langmuir* **2004**, *20* (2), 416–422.
(37) Baklanov, M. R.; Mogilnikov, K. P.; Polovinkin, V. G.; Dultsev, F. N. Determination of pore size distribution in thin films by ellipsometric porosimetry. *J. Vac. Sci. Technol., B: Microelectron. Nanometer Struct.—Process., Meas., Phenom.* **2000**, *18* (3), 1385–1391.
(38) Lukens, W. W.; Schmidt-Winkel, P.; Zhao, D.; Feng, J.; Stucky, G. D. Evaluating pore sizes in mesoporous materials: Simplified standard adsorption methods and a simplified Broekhoff−de Boer method. *Langmuir* **1999**, *15*, 5403–5409.
(39) Palik, E. D. *Handbook of Optical Constants*; Academic Press: San Diego, 1985; Vol. 1.

pressure of toluene was controlled using two mass flow controllers (MKS) for saturated toluene and air streams. This mixed stream then flowed through a custom built cell with fixed fused silica windows. Both adsorption and desorption isotherms were measured. To calculate the PSD, the EP data were analyzed on the basis of the change in refractive index as a function of relative toluene pressure.[37]

The porosity of the film also can be calculated from the EP data without assumptions about the silica wall refractive index. Since the mesoporous film contains wall material and voids, two unknowns exist in the Bruggemann effective medium approximation (n_{wall} and P). However, if all the pores are filled when exposed to saturated vapor (generally a good assumption), a second equation with the same two unknowns is obtained if the optical constants for the condensed probe solvent is known (assuming bulk refractive index in the mesopores). Thus, from these two equations, both the porosity and the refractive index of the wall material were calculated using the Bruggemann EMA model. Additionally, saturated water also was used as a probe to calculate the total film porosity for comparison to the porosity determined from toluene adsorption.

Results and Discussion

Changes in Film Properties during Synthesis. The reaction within the template film was assessed by examining changes in the film thickness and refractive index after each step in the film processing. In particular, three specific film types were measured using ellipsometry: the polymer template, silica-polymer nanocomposite, and mesoporous silica. To avoid any film thickness effects, all template films were initially approximately 590 nm thick. Additionally, the reaction conditions were chosen to avoid any dramatic changes from T_g depression by CO_2 TEOS and water sorption,[40] which could lead to orders of magnitude changes in the transport properties but would be processing dependent. The blend template utilized here was rubbery at 60 °C, which avoids ambiguities. Changing to a glassy template would enhance any transport limitations present in the vapor based synthesis.

The condensation of TEOS within the template film resulted in film swelling that was controlled by the extent of reaction. By simply exposing the template to the vapor pressure of TEOS and water, the film thickness increased significantly from 590 nm to nearly 1200 nm after 30 min of reaction. In this case, the nanocomposite film was mostly inorganic silica, and transport of the precursors through the entire film thickness was possible during synthesis. This suggests that the transport limitations of the precursors were insufficient to prevent the formation of a continuous film (i.e., the reaction occurred through the full thickness of the polymer film) for a rubbery template using vapor exposure. On the basis of prior arguments that SC-CO_2 increases the diffusivity of the precursors through the template film, even greater swelling extents from the condensation reaction would be expected at higher pressures, as the reactants can diffuse quickly through the template. Comparison of the vapor phase and low CO_2 pressure (36 bar) reaction shows a small increase in the film thickness upon the introduction

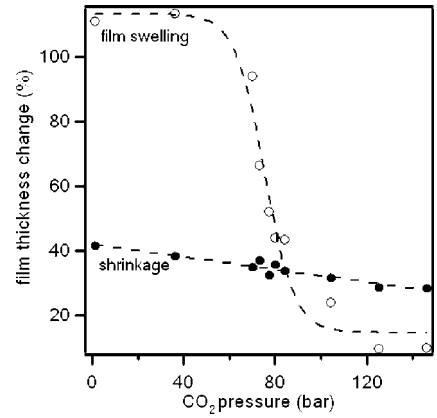

Figure 1. Film thickness (○) swells during reaction due to the incorporation of silica into the polymer matrix. Film swelling decreases dramatically once the reaction pressure exceeds the CO_2 critical pressure (73.8 bar). Calcination (•) leads to film shrinkage that decreases slightly as the CO_2 pressure increases.

of CO_2. However, as illustrated in Figure 1, as the reaction CO_2 pressure is increased, the ultimate film thickness changes from the reaction decrease significantly. This decreased swelling is most pronounced near P_c ($P_c = 73.8$ bar). There are a number of explanations for this behavior, including a change in the rate limiting step of the reaction diffusion process, a change in the reaction kinetics, and/or the varying solubility of the TEOS in the template, which is a function of CO_2 pressure. Near the critical point, the reaction rate of several homogeneous reactions is known to decrease significantly.[41] Combined with the increased diffusivity of small molecules within the polymer film as the CO_2 pressure increases,[42] this reaction rate change also could change the mechanism from diffusion limited to reaction limited; however, since the reaction is occurring within a polymer-CO_2 swollen phase, it is highly unlikely that the critical point for the mixture is the same as for neat CO_2. A more likely scenario is that the relative affinity of TEOS is greater toward the CO_2 phase than the polymer phase.

The solvent quality of CO_2 increases with increasing pressure. Therefore, the equilibrium TEOS concentration within the template film will decrease as the CO_2 pressure is increased. For the reactive case examined here, the decrease in TEOS solubility in the template will decrease the amount of silica formed through simultaneously decreasing the driving force for diffusion and reaction. This effect is similar to that observed for the infusion of small molecules into polymers using CO_2; this is simply driven by the partitioning of the additive between phases.[43] In the present case, due to reaction within the polymer phase that continuously depletes the additive, the analysis is more complex.[44,45] As the solubility of TEOS in CO_2 is substantial (in excess of 30% at moderate conditions),[46] partitioning of TEOS to the CO_2 phase as the pressure is increased is expected. Moreover, the solubility of many organic compounds in CO_2

(40) Wissinger, R. G.; Paulaitis, M. E. Glass transitions in polymer CO_2 mixtures at elevated pressures. *J. Polym. Sci., Part B: Polym. Phys.* **1991**, *29* (5), 631–633.

(41) Brennecke, J. F.; Chateauneuf, J. E. Homogeneous organic reactions as mechanistic probes in supercritical fluids. *Chem. Rev.* **1999**, *99* (2), 433–452.

(42) Gupta, R. R.; Ramachandra Rao, V. S.; Watkins, J. J. Measurement of probe diffusion in CO_2-swollen polystyrene using in situ fluorescence nonradiative energy transfer. *Macromolecules* **2003**, *36* (4), 1295–1303.

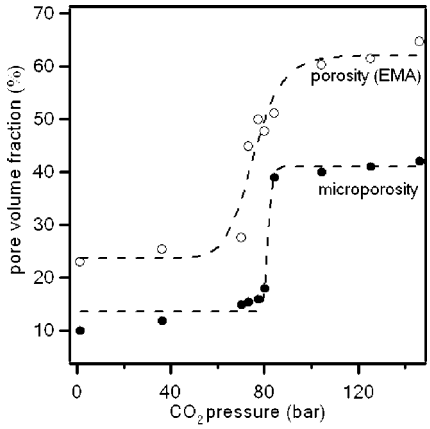

Figure 2. Total porosity of films determined using the EMA model from ellipsometry data is shown by open symbols (○). Microporosity is shown by closed symbols (•). The porosity increases significantly as the CO_2 pressure increases from below P_c to above P_c.

increases significantly as the pressure is increased above P_c.[47] A decreased solubility of TEOS within the template film would tend to decrease the reaction rate. Similar trends with CO_2 pressure for the infusion and polymerization of styrene within a homopolymer matrix have been observed previously.[48] The nanocomposite film synthesized at 146 bar only swelled by 9.9% in comparison to a nearly 115% increase when the CO_2 pressure was 36 bar. Because of the similarity of the refractive index between silica and most polymers, no significant changes in the refractive index for all films were evident from the TEOS condensation within the template film.

However, upon calcination, the refractive index of the film decreased tremendously. The decrease in the refractive index resulted from the formation of pores within the silica matrix templated by the amphiphilic polymer. This change in refractive index was utilized to calculate the total porosity of the films using the EMA.[39] Figure 2 illustrates the substantial increase in porosity as the reaction pressure increases. Similar to the thickness change during the reaction, there is a near step change in properties near P_c. Synthesis below P_c yields films with porosities near 25%, and the porosity increases to approximately 45% just above P_c. As the pressure further increases, the porosity of films doubles from the low pressure regime to approximately 60%. Thus, the total porosity of the silica films is substantially influenced by the pressure of CO_2. This is not unexpected given the extent of reaction within the films; less silica will generally result in a larger porosity.

In addition to the decrease in refractive index following calcination, the film thickness also decreased predominately due to incomplete network formation during the condensation reaction.[27] For the films examined here, the shrinkage of the film decreased as the CO_2 reaction pressure increased (Figure 1). Vapor pressure condensation resulted in approximately 42% shrinkage during calcination, but the film synthesized at 146 bar only contracted 28%. These results suggest that CO_2 enhances network formation. This can be rationalized using Le Chatelier's principle; ethanol is a byproduct of the condensation reaction that accumulates in the template due to favorable interactions, but ethanol is also very soluble in CO_2. Thus, synthesis in CO_2 extracts the ethanol byproduct and drives the condensation reaction forward.

Mesoporous Film Structure. The ellipsometry measurements only confirm that the films are porous. However, these measurements do not provide any information about the pore size or the pore morphology. Here, XRD was utilized to ascertain the structure of the films. The 1-D diffraction patterns from the films are shown in Figure 3a. At least one diffraction peak is present for all the films, indicative of the length scale templated by Pluronic. Most of these films appear to be highly ordered as evidenced by multiple diffraction peaks. The peak position ratio from diffraction is approximately $1:\sqrt{2}:2$, which is indicative of a bcc structure ($Im\bar{3}m$). However, at high pressures (>100 bar), the ordering of the mesopores appears to degrade as only one diffraction peak is present. As discussed later, TEM confirms the presence of a bcc structure for all of the films. The breadth of the diffraction peak also can be used to estimate the degree of ordering through the film.[49] Analogous to the diffraction of small metal crystals, the Bragg peak width is inversely proportional to the grain size of the ordered mesopores. A narrower diffraction peak is thus indicative of improved long-range order of the mesopores. Table 1 shows as to how CO_2 conditions during synthesis impact the width of the Bragg reflection and hence the ordering of the mesoporous silica. The long-range ordering improves as the CO_2 pressure increases at low pressure (<84 bar) with a narrowing of the Bragg reflection. The film synthesized at 84 bar has the narrowest peak width, which suggests that this condition yields the most ordered structure. This is confirmed with cross-sectional TEM (Figure 4), which shows larger grains for the film synthesized at 84 bar. However, as the CO_2 pressure increases, the width of the Bragg reflection is tremendously increased, which corresponds to smaller grains and thus a shorter range order of the mesopores.

Interestingly, the primary peak position does not appreciably shift as a result of CO_2 pressure. The primary diffraction peak provides the average spacing between pore centers. On the basis of the significant differences in porosity and reaction extent determined from ellipsometry, one would assume that the pore wall thickness would change significantly such that the diffraction peak position would abruptly shift to higher angles as the pressure during synthesis was

(43) Berens, A. R.; Huvard, G. S.; Korsmeyer, R. W.; Kunig, F. W. Application of compressed carbon dioxide in the incorporation of additives into polymers. *J. Appl. Polym. Sci.* **1992**, *46* (2), 231–242.
(44) Watkins, J. J.; Mccarthy, T. J. Polymerization in supercritical fluid-swollen polymers—A new route to polymer blends. *Macromolecules* **1994**, *27* (17), 4845–4847.
(45) Watkins, J. J.; Mccarthy, T. J. Polymer/metal nanocomposite synthesis in supercritical CO_2. *Chem. Mater.* **1995**, *7* (11), 1991–1994.
(46) Brown, G. D.; Watkins, J. J. Materials issues and modeling for device nanofabrication. *Mater. Res. Soc. Symp. Proc.* **2000**, *584*, 169.
(47) Johnston, K. P.; Ziger, D. H.; Eckert, C. A. Solubilities of hydrocarbon solids in supercritical fluids—The augmented van der Waals treatment. *Ind. Eng. Chem. Fundam.* **1982**, *21* (3), 191–197.
(48) Watkins, J. J.; Mccarthy, T. J. Polymerization of styrene in supercritical CO_2—swollen poly(chlorotrifluoroethylene). *Macromolecules* **1995**, *28* (12), 4067–4074.
(49) Vogt, B. D.; Lee, H. J.; Wu, W. L.; Liu, Y. F. Specular X-ray reflectivity and small angle neutron scattering for structure determination of ordered mesoporous dielectric films. *J. Phys. Chem. B* **2005**, *109* (39), 18445–18450.

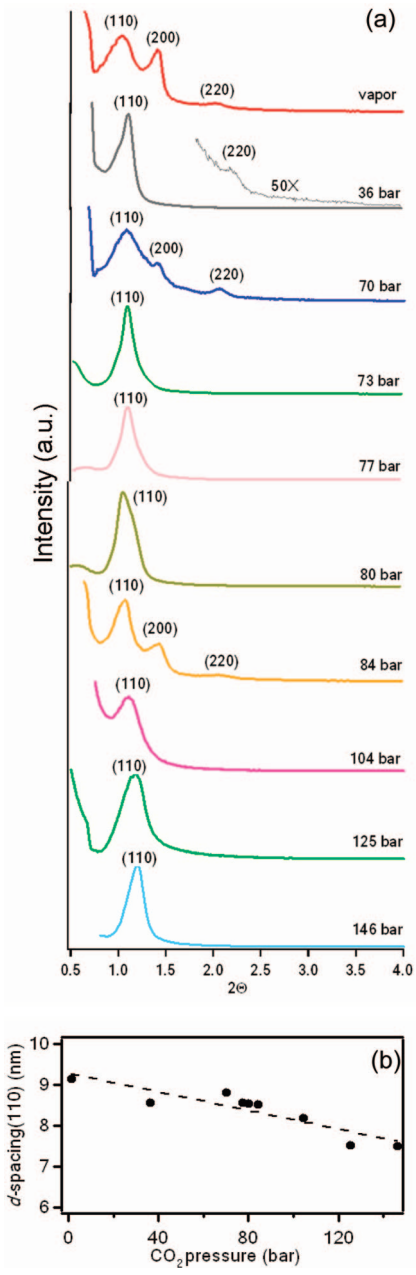

Figure 3. (a) Influence of CO_2 pressure on X-ray diffraction profiles of calcined mesoporous silica. The peaks are identified as (110), (200), and (220) for a cubic structure $Im\bar{3}m$. (b) The *d*-spacing (110) as determined from Bragg's law decreases as the CO_2 pressure is increased.

increased beyond P_c. Instead, there was only a small shift in the primary peak position from 1.03 to 1.2° as the CO_2 pressure increased from 0 to 146 bar. The resulting *d*-spacing (110) is shown in Figure 3b. To accurately calculate the *d*-spacing, the diffraction peak position was corrected for refraction by using the critical angle of the sample.[21] The critical angle, α_c, is calculated from the porosity of the sample and assuming that the silica wall density is 2.2 g/cm^3.[21] The *d*-spacing (110) decreases nearly linearly from 9.15 to 7.51 nm as the CO_2 pressure increases. This result is contrary to expectations based upon the step change in the porosity of the films synthesized near P_c and suggests that there is a large increase in pore size near the critical pressure.

TEM was used to confirm the structure of the films and to determine the pressure dependence of pore size. Previous studies have indicated a surface capping layer for films synthesized with vaporized precursors.[21] Here, without homogeneous condensation in the vapor phase, there is still a surface layer on top of the mesoporous films formed by this vapor exposure as illustrated in Figure 4a. This means that although the precursors are able to diffuse through the film thickness (as evidenced by the well-ordered mesopores near the substrate surface), transport limitation exists to create a gradient in film properties near the surface of the film. An approximately 30 nm thick capping layer still remains even for a CO_2 pressure up to 36 bar (Figure 4b). As the CO_2 pressure is further increased, this surface coating is eliminated as illustrated in Figure 4. This observation is consistent with the increase in precursor diffusivity in the template from the sorption of CO_2. Additionally, the film formation process requires both diffusion and reaction. A decrease in the equilibrium concentration of TEOS within the template as the CO_2 pressure is increased would lead to a decrease in the condensation rate as well. Both effects would tend to create a more homogeneous nanostructure, consistent with the TEM results for SC-CO_2 synthesized films. Moreover, solvents tend to disorder the mesostructure of block copolymers.[50–52] The solubility of TEOS vapor within the template is substantial as a film not containing p-TSA (no condensation) appears to be "wet" after exposure. In examining the surface layer formed from vapor exposure (see Figure 5), the surface layer contains some small disordered and distorted pores; this is also consistent with a high TEOS concentration at the film surface, leading to dissolution of the template and the formation of a disordered, mildly porous silica surface layer from subsequent TEOS condensation.

In examining the nanostructure, all films synthesized below 104 bar have a well-defined $Im\bar{3}m$ mesostructure with a surface layer only present at low pressures with large areas of well-ordered spherical pores. For the film synthesized at 70 bar, the pore radius is 1.91 nm and the *d*-spacing (110) is 9.34 nm from the micrograph. This *d*-spacing agrees well with the *d*-spacing (110) value calculated from the corresponding XRD pattern (8.82 nm). The *d*-spacing for the film synthesized at 84 bar decreased to approximately 8.55 nm from TEM, which is similar to the *d*-spacing (110) value calculated from the XRD result. However, the pore radius increased tremendously from 1.91 to 3.98 nm. This indicates that the mesopore size increased tremendously for films synthesized using SC-CO_2 (i.e., $P > P_c$). However, at higher pressures ($P >$ 125 bar), a degradation in the ordering of the films was observed.

Although CO_2 can lead to disordering of block copolymers, it is unlikely that the poor order in films synthesized at high pressure is due to a CO_2 solvation effect. Highly ordered mesoporous silica films have been reported previously at similar conditions (*T* and *P*).[24] However,

(50) Lodge, T. P.; Hanley, K. J.; Pudil, B.; Alahapperuma, V. Phase behavior of block copolymers in a neutral solvent. *Macromolecules* **2003**, *36* (3), 816–822.
(51) Lodge, T. P.; Pudil, B.; Hanley, K. J. The full phase behavior for block copolymers in solvents of varying selectivity. *Macromolecules* **2002**, *35* (12), 4707–4717.
(52) Guenza, M.; Schweizer, K. S. Local and microdomain concentration fluctuation effects in block copolymer solutions. *Macromolecules* **1997**, *30* (14), 4205–4219.

Table 1. Morphological Characteristics of Mesoporous Films as a Function of CO_2 Pressure

silica film	porosity (%) (EMA, assumed silica *n*)	porosity (%) (EMA, toluene sorption)	*d*-spacing (nm) (XRD)	primary peak width (XRD)	av pore radius (nm) (TEM)	av pore radius (nm) (desorption)	av pore radius (nm) (adsorption)
vapor	23.1	16.7	9.2	0.15	1.9	1.6	4.7
36 bar	25.5	22.4	8.6	0.15	1.9	1.7	7.0
70 bar	27.7	24.6	8.8	0.18	1.9	1.8	5.7
73 bar	45	51.5	9.5	0.12		1.8	4.7
77 bar	50.1	43.9	8.6	0.12		1.8	3.3
80 bar	47.8	62.1	8.6	0.14		1.8	3.6
84 bar	57.2	19.2[a]	8.5	0.10	4.0	3.9	5.8
104 bar	60.3	38.2[a]	8.2	0.22	3.7	3.7	6.8
125 bar	61.5	49.2[a]	7.5	0.17	3.6	3.8	9.0
146 bar	64.8	36.7[a]	7.5	0.15	3.8	3.9	7.2

[a] Pores appear to be only partially accessible.

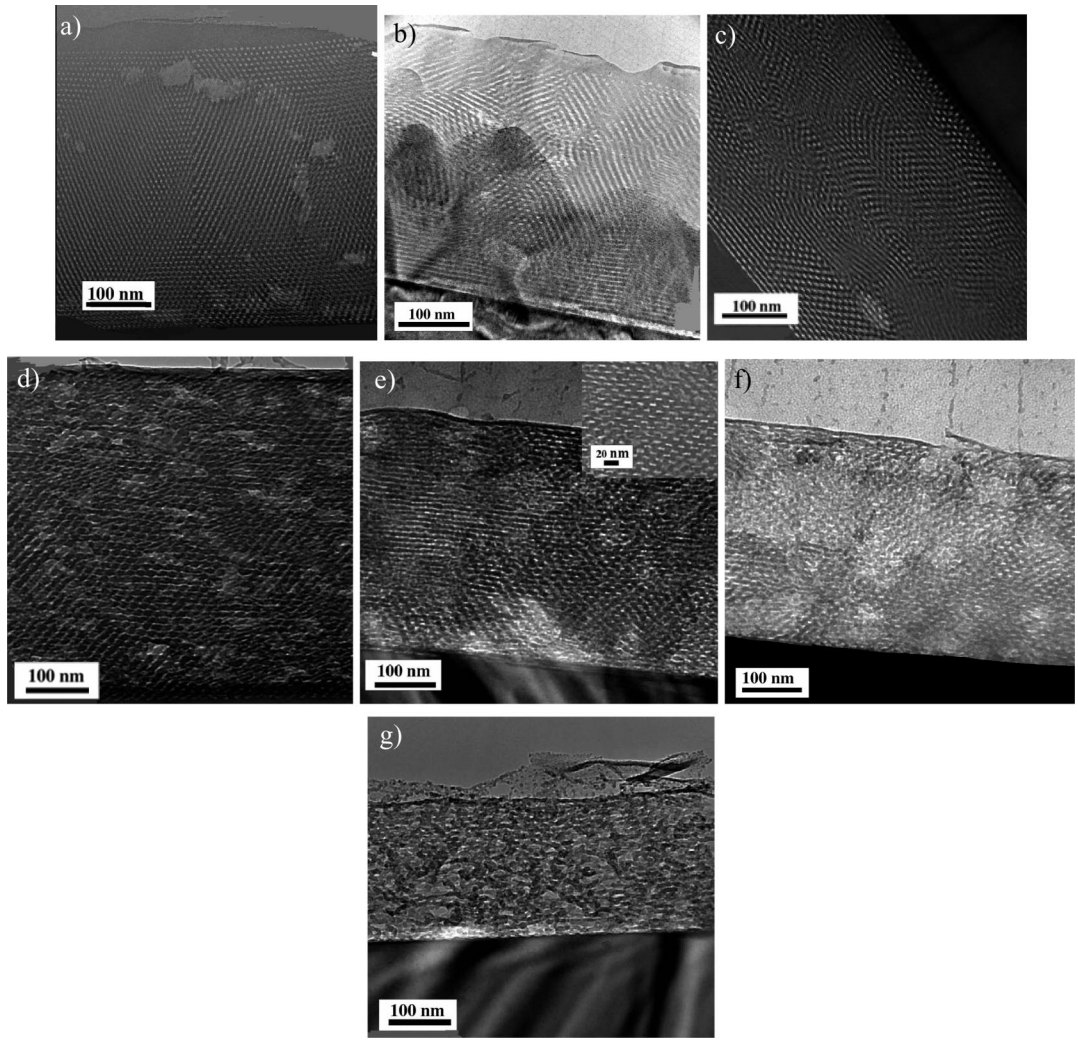

Figure 4. Transmission electron micrographs of calcined mesoporous silica films synthesized using (a) vapor exposure or CO_2 at (b) 36 bar, (c) 70 bar, (d) 84 bar, (e) 104 bar, (f) 125 bar, and (g) 146 bar. The pores in the film prepared at below P_c are approximately half of the size as compared to the film synthesized above P_c.

the TEOS concentration in the CO_2 phase was probably significantly larger. The TEOS concentration will impact its partitioning and also the reaction rate within the template. For the specific fixed TEOS volume fraction examined in this work, the amount of silica formed within the template at these high pressures was minimal. We hypothesize that the stresses induced during calcination are sufficient to distort the pore structure, leading to the observed poor ordering. The CO_2 pressure threshold for degrading the order of the mesopores is likely strongly dependent upon the initial TEOS loading; similarly, the pressure required to eliminate the silica surface layer also should be dependent upon the TEOS concentration in the CO_2 phase, which will define the TEOS partitioning between the fluid and the polymer template phases.

Pore Size Distribution. To quantify as to how CO_2 pressure influences the pore size in mesoporous silica films, EP was utilized to elucidate the pore size distribution using toluene vapor as the probe molecule. Adsorption and desorption isotherms were obtained by monitoring changes

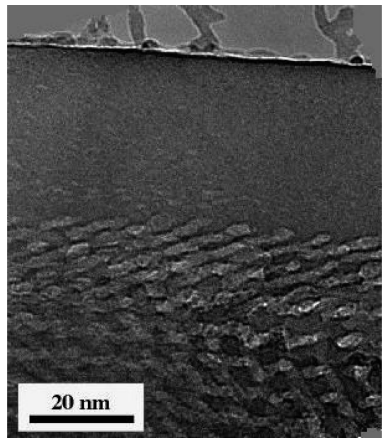

Figure 5. TEM cross-section micrograph of the top layer in a calcined silica film prepared with vapor exposure. The surface layer is slightly porous.

in the refractive index of the film upon exposure to varying partial pressures of toluene. Capillary condensation of toluene within the pores led to a significant increase in the average refractive index of the film as illustrated in Figure 6. For all adsorption isotherms, the refractive index of the film initially increased slowly as the partial pressure was increased, corresponding to the filling of the small micropores templated by the PHOSt and PEO segments of F108.[4,5,27] At some critical intermediate partial pressure, there was a dramatic increase in the refractive index corresponding to the filling of the mesopores. Desorption from these mesopores did not occur reversibly, but rather, lower pressures were required. This hysteresis is commonly observed in BET and EP measurements of mesoporous films and is attributed to the "ink-bottle" effect.[53] In the micropore regime, some adsorption and desorption curves did not crossover at the end of the desorption process. This slight difference commonly was observed for toluene sorption in mesoporous silicates and does not appear to be associated with kinetic limitations in the desorption.[54] From the shape of the adsorption and desorption isotherms, it is possible to estimate the fraction microporosity within each film by assuming that mesopore filling only occurs in the hysteresis loop.[27] For films synthesized below P_c, the microporosity is between 10 and 15% of the total porosity, which is similar to the silica films synthesized with the EISA method.[55] However, a significant increase in the microporosity was observed for the mesoporous films processed with SC-CO_2, with almost 40% of total porosity being micropores, consistent with previous studies of mesoporous organosilicate films synthesized with SC-CO_2.[27]

The pore size distribution (PSD) for each film was determined from the desorption isotherm using the Kelvin equation. The mesopore radius was calculated as $r_p = r_k + t$, where r_k is the Kelvin radius and t is the thickness of the adsorbed layer of vapor in the pores before capillary condensation occurs.[37] The Kelvin equation relates the size of a filled pore to the partial pressure and physical properties of an adsorbing gas as

$$\ln \frac{p}{p_0} = -\frac{2\gamma V_m}{r_k RT} \tag{1}$$

where p is the vapor pressure, p_0 is the saturated vapor pressure, γ is the surface tension of the adsorbing species, V_m is the adsorbate molar volume in the condensed state, r_k is the Kelvin radius, R is the gas constant, and T is temperature. The thickness of the adsorbed toluene layer t defined by the BET equation is based upon the published adsorbed thickness on nonporous silica as[37]

$$t = \frac{d_0 CK(P/P_0)}{[1 - K(P/P_0)][1 + K(C-1)(P/P_0)]} \tag{2}$$

where d_0 is the thickness of a toluene monolayer on silica (0.37 nm).[56] C is the BET constant $C = \exp[(q_1 - q_L)/RT]$, where q_1 and q_L are the heat of adsorption in the first monolayer and the molar heat of condensation.[57] C is estimated as 289.1 at room temperature based upon published heats of adsorption and condensation for toluene on silica.[57] K (0.8) is a coefficient that satisfies the requirement that at $P = P_0$, $t \leq$ 5–6 monolayers.[53] To correct for the discrete number of points involved in the measurement of toluene sorption isotherms, each isotherm was fit to an arbitrary function based upon a series of Gaussian and sigmodial functions[58] to calculate the PSD for each film as illustrated in Figure 6b. Two distinct distributions of pores are present in most samples: a broad distribution of small micropores templated by the hydrophilic PHOSt and PEO segments of F108 and a relatively narrow distribution of mesopores between 2 and 4 nm templated by the hydrophobic PPO segments.

Consistent with the TEM micrographs, the average mesopore size in the vicinity of P_c becomes significantly larger as shown in Table 1. The pore radius more than doubles as the reaction pressure increases from 70 bar (1.8 nm) to 84 bar (3.9 nm). Figure 7 clearly illustrates the discontinuity in pore radii near P_c. This significant pore size change is distinctive from the data of Holmes and co-workers on the pore expansion of ordered silica nanocomposites with CO_2, which linearly increases with the CO_2 pressure.[28,29] The origins of the substantial increase in pore size near P_c is unclear but is suspected to be a result of changes in the solvent strength of CO_2 and subsequent partitioning of TEOS between CO_2 and polymer phases. The solubility of CO_2 in poly(ethylene oxide) is a smooth function of pressure and cannot be used to explain the more than 100% increase in pore size in crossing the critical pressure.[59]

(53) Gregg, S. J.; Sing, S. W. *Adsorption, Surface Area, and Porosity*; Academic Press: London, 1982.
(54) Bourgeois, A.; Bruneau, A. B.; Fisson, S.; Demarets, B.; Grosso, D.; Cagnol, F.; Sanchez, C.; Rivory, J. Determination of pore size distribution in thin organized mesoporous silica films by spectroscopic ellipsometry in the visible and infrared range. *Thin Solid Films* **2004**, *447*, 46–50.
(55) Deng, Y. H.; Yu, T.; Wan, Y.; Shi, Y. F.; Meng, Y.; Gu, D.; Zhang, L. J.; Huang, Y.; Liu, C.; Wu, X. J.; Zhao, D. Y. Ordered mesoporous silicas and carbons with large accessible pores templated from amphiphilic diblock copolymer poly(ethylene oxide)-*b*-polystyrene. *J. Am. Chem. Soc.* **2007**, *129* (6), 1690–1697.
(56) Koselev, A. V.; Khopina, V. V.; El'tekov, I. A. Adsorption of toluene−heptane mixtures on silica gels and carbon blacks. *Russ. Chem. Bull.* **1958**, *7* (6), 647–653.
(57) Choudhary, V. R.; Mantri, K. Adsorption of aromatic hydrocarbons on highly siliceous MCM-41. *Langmuir* **2000**, *16* (17), 7031–7037.
(58) Lee, H. J.; Soles, C. L.; Liu, D. W.; Bauer, B. J.; Lin, E. K.; Wu, W. L.; Grill, A. Structural characterization of porous low-*k* thin films prepared by different techniques using X-ray porosimetry. *J. Appl. Phys.* **2004**, *95* (5), 2355–2359.

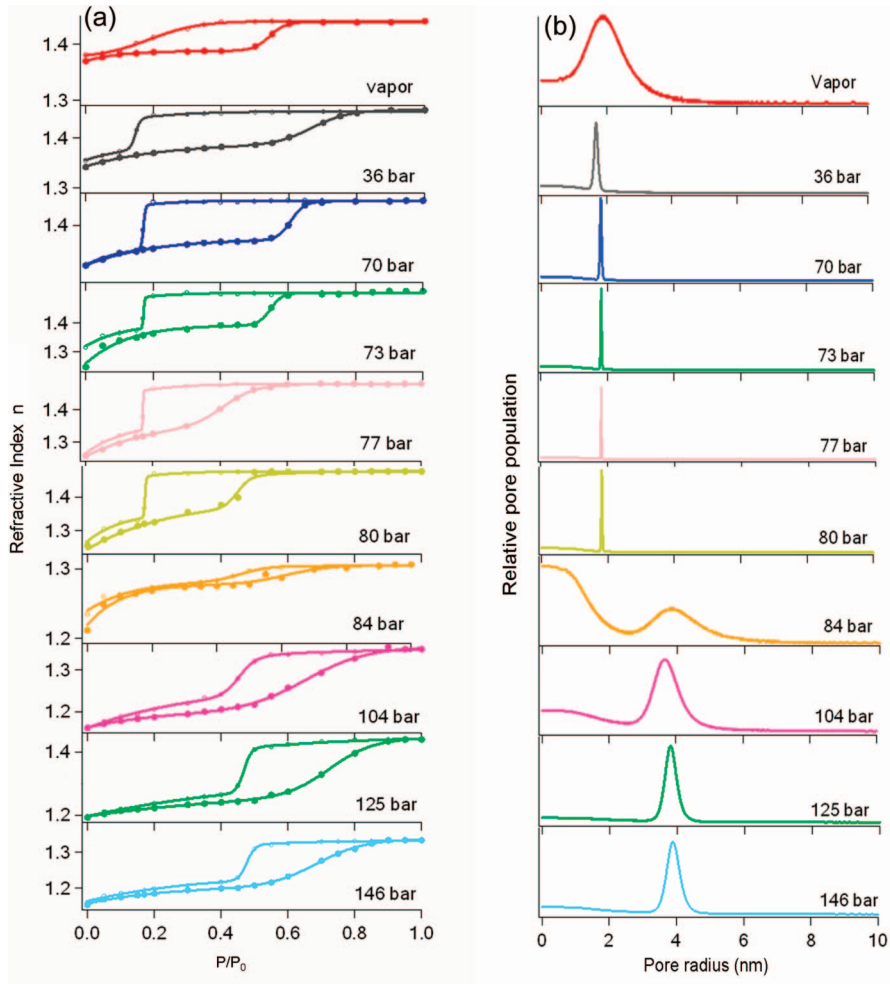

Figure 6. (a) Adsorption and desorption isotherms for toluene in mesoporous silica films as determined by the changes in the refractive index ($\lambda = 632$ nm) of the silica film as a function of the adsorbate (toluene) relative pressure and pore size distribution. (b) Calculated pore size distribution based upon the desorption branch of the isotherms.

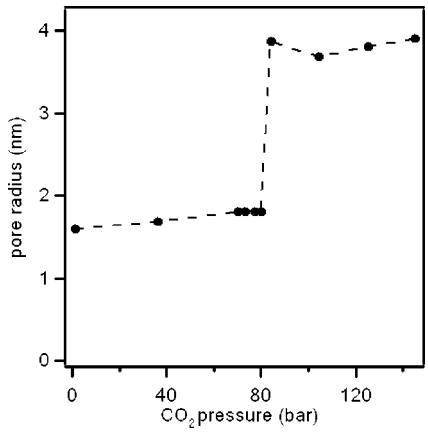

Figure 7. Average pore radius of the mesoporous films as a function of CO_2 pressure. Pore radius slightly increases with CO_2 pressure at $P < P_c$, but a discontinuity in the pore radius occurs near P_c with the pore size more than doubling.

One additional anomaly from these adsorption/desorption isotherms is that for samples synthesized at pressures above P_c, the refractive index for the films exposed to saturated toluene vapor is significantly decreased. This is unexpected as the refractive indices for toluene and silica are similar ($n_{silica} = 1.458$[39] and $n_{toluene} = 1.497$[54]). Thus, if all the pores are filled with toluene, the refractive index should be between 1.458 and 1.497. However, for SC-CO_2 based syntheses, the refractive index upon exposure to saturated toluene vapor is significantly less. This indicates that some pores are unfilled by toluene and potentially inaccessible. Thus, the porosity calculated using the Bruggemann EMA equation to calculate the porosity and silica refractive index from the unfilled and filled films will be inaccurate. For films synthesized at a CO_2 pressure of <80 bar, the porosity calculated with the EMA model (assumed silica wall refractive index) agrees well with the porosity calculated with the Bruggemann EMA equation using the refractive index of the films with empty pores and toluene filled pores (Table 1).[60] This result indicates that all pores are filled with condensed toluene in these films as would be expected. Conversely, for films synthesized above 70 bar, the calculated porosities by these two methods are not comparable. The final refractive index obtained in saturated toluene is still quite low (<1.35) for films synthesized at 84, 104, and 146 bar, which indicates that

(59) Hata, K. The sorption properties of supercritical carbon dioxide in poly(ethylene glycol) and poly(ethylene oxide) with high pressure thermogravimetry-differential thermal analysis. *Kobunshi Ronbunshu* **2001**, *58* (12), 714–717.
(60) Boissiere, C.; Grosso, D.; Lepoutre, S.; Nicole, L.; Bruneau, A. B.; Sanchez, C. Porosity and mechanical properties of mesoporous thin films assessed by environmental ellipsometric porosimetry. *Langmuir* **2005**, *21* (26), 12362–12371.

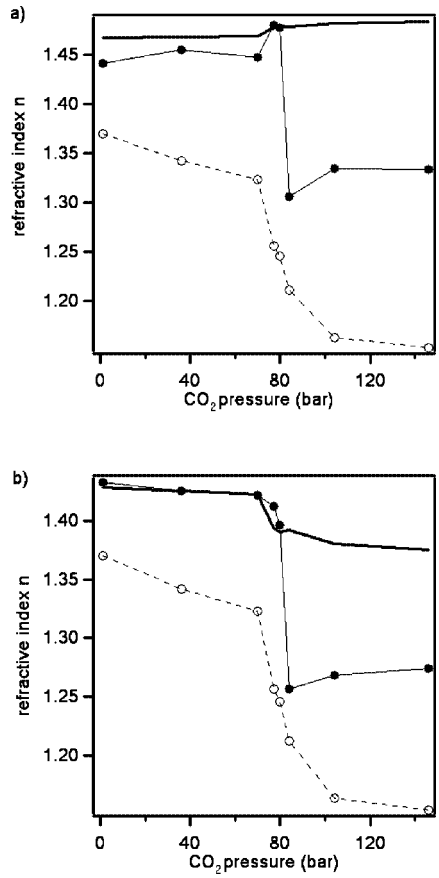

Figure 8. Refractive index, n, of mesoporous silica films exposed to (a) saturated toluene and (b) water measured using EP. The refractive index of the neat (empty pores) mesoporous silica (○) decreased with a CO_2 pressure increase. The refractive index after saturated solvent exposure (•) increased due to capillary condensation within the mesopores. Experimentally measured n agrees well with refractive index calculated based upon a fixed silica wall refractive index and total pore filling (—) when $P < P_c$. When the films are synthesized at $P > P_c$, significant deviations arise, suggesting inaccessible pores.

only a portion of the pores is filled as shown in Figure 8. This reproducible phenomenon could be rationalized to result from isolated pores in the films that are not accessible to small molecules, such as toluene. According to the difference between the porosity calculated with the EMA model and the Bruggemann equation, almost 65% of the total pore volume is not filled by toluene for the film processed at 84 bar. Pore accessibility becomes extremely low in the vicinity of P_c. On the basis of prior reports, all pores in mesoporous silica films should be accessible to toluene.[54]

To test for specific chemical and size effects, water also was employed as a probe molecule to check for pore filling (accessibility) of these mesoporous silica films. Water has a smaller molecule size than toluene and thus can be used to check for finite size effects on the accessibility. Similar to the results for toluene, pores in films processed above 84 bar were not completely filled upon exposure to saturated water vapor. The origins of this limited accessibility are unclear. However, there is a significant increase in the micropore fraction within the films synthesized above the critical pressure. Typically, these micropores should enhance transport of small molecules, and hence, condensation within the mesopores should be facilitated. However, the micropores could roughen the walls of the mesopores to create a non-wetting surface that would prevent condensation within the mesopores as surface roughness is a key parameter for the wetting of planar surfaces.[61] For microelectronic applications, internally connected pores in most mesoporous materials provide pathways for the penetration of condensable gases, liquids, or even solid particles that can lead to deterioration of mechanical, electrical, and thermal properties during chemical mechanical treatments.[62,63] Films synthesized at $P > P_c$ are attractive as low-k materials as liquid contamination issues[62,63] may be alleviated due to limited pore accessibility to small molecules.

Conclusion

The influence of CO_2 on the synthesis of mesoporous silica films was examined systematically as a function of pressure. At low pressures, transport limitations within the polymer template and high precursor concentrations led to the formation of a skin layer and a gradient in porosity near the film surface. Changes in the film thickness during processing illustrate a discontinuity in the properties near P_c. Below P_c, the average mesopore size increases linearly with CO_2 pressure in accordance with simple polymer sorption. However, the pore size more than doubles when the synthesis conditions change from gaseous to supercritical for CO_2. Additionally, the porosity of the film increased substantially for films synthesized using SC-CO_2. Surprisingly, these highly porous films have a significant percentage that is inaccessible to small molecules (toluene and water) as evidenced by limited condensation within the pores. High porosity films with spherical mesopores that are inaccessible to water may be particularly important for the fabrication of ultralow dielectric constant films to overcome contamination issues for integration.

Acknowledgment. The authors acknowledge financial support from the State of Arizona and the National Science Foundaiton under CBET-0746664. We thank DuPont Electronic Materials (Jim Sounik and Michael Sheehan) for the donation of poly(4-hydroxystyrene). We acknowledge the use of facilities in the LeRoy Eyring Center for Solid State Science. The authors thank Jerry Y. S. Lin for access to XRD instrumentation.

CM8003479

(61) Chen, W.; Fadeev, A. Y.; Hsieh, M. C.; Oner, D.; Youngblood, J.; Mccarthy, T. J. Ultrahydrophobic and ultralyophobic surfaces: Some comments and examples. *Langmuir* **1999**, *15* (10), 3395–3399.
(62) Abell, T.; Maex, K. Damage minimized plasma pore sealing of microporous low k dielectrics. *Microelectron. Eng.* **2004**, *76* (1–4), 16–19.
(63) Maex, K.; Baklanov, M. R.; Shamiryan, D.; Iacopi, F.; Brongersma, S. H.; Yanovitskaya, Z. S. Low dielectric constant materials for microelectronics. *J. Appl. Phys.* **2003**, *93* (11), 8793–8841.